Numerical modeling of coanda effect in a novel propulsive system

Shyam S. Das[a*], M. Abdollahzadeh[a], Jose C. Pascoa[a], A. Dumas[b], M. Trancossi[b]

[a]Department of Electromechanical Engineering, Center for Mechanical and Aerospace Sciences and Technology, University of Beira Interior, R. Mq.s D´Ávila e Bolama, 6201-001 Covilhà, Portugal

[b]Dipartimento di Scienze e Metodi dell'Ingegneria Università di Modena e Reggio Emilia, 42122 Reggio Emilia, Italy

ABSTRACT

Coanda effect (adhesion of jet flow over curved surface) is fundamental characteristics of jet flow. In the present paper, we carried out numerical simulations to investigate Coanda flow over a curved surface and its application in a newly proposed Propulsive system "A.C.H.E.O.N" (Aerial Coanda High Efficiency Orienting jet Nozzle) which supports thrust vectoring. The ACHEON system is presently being proposed for propelling a new V/STOL airplane in European Union. This system is based on cumulative effects of three physical effects such as (1) High speed jet mixing speeds (2) Coanda effect control by electrostatic fields (3) Coanda effect adhesion of an high speed jet to a convex surface. The performance of this nozzle can be enhanced by increasing the jet deflection angle of synthetic jet over the Coanda surface. This newly proposed nozzle has wide range of applications. It can be used in industrial sector such as plasma spray gun and for direct injection in combustion chamber to enhance the efficiency of the combustion chamber. Also, we studied the effect of Dielectric barrier discharge (DBD) plasma actuators on A.C.H.E.O.N system. Dielectric barrier discharge (DBD) plasma actuators are active control devices for controlling boundary layer and to delay the flow separation over any convex surfaces. Computations were performed under subsonic condition. Two dimensional CFD calculations were carried out using Reynolds averaged Navier stokes equations (RANS). A numerical method based on finite volume formulation (FVM) was used. SST k-ω model was considered to model turbulent flow inside nozzle. DBD model was used to model the plasma. Moreover, a body force treatment was devised to model the effect of plasma and its coupling with the fluid. This preliminary result shows that, the presence of plasma near Coanda surface accelerates the flow and delays the separation and enhances the efficiency of the nozzle.

Keywords: Coanda effect, ACHEON system, thrust vectoring, plasma, combustion, turbulence model,

1. INTRODUCTION

Air transport has completely transformed our society in the last 100 years. The excess use of air transport leads to development of Vertical Short-Take off and Landing (V/STOL) air vehicles in the modern world. These types of air vehicles have enormous operational

*corresponding author

advantages in field of military, humanitarian and rescue operations. V/STOL aircrafts based on thrust vectoring. Thrust vectoring is the ability of an aircraft or other vehicle to deflect the angle of its thrust away from the vehicles longitudinal axis [41]. Further, the use of thrust vectoring concept enables to control the aircraft in more controllable way. In case of military operations it can introduce an extension on aircraft controllability at high post angle of attacks, a moment where classic lifting surface lose their ability to provide the control of aircraft, creating what is called super maneuverability [45]. This technology will improve take off and landing performances. It will allow the exploration of radical new concepts of aerial vehicle design realizing advanced concepts which have been previously postulated throughout the history of aviation but could not be realized because of the lack of an effective and affordable jet vectoring system. ACHEON (Aerial Coanda High Efficiency Orienting jet Nozzle) explores the feasibility of a novel propulsive system for aircraft which is expected to overcome the main limitations of traditional systems related to typical jet deflection systems [1, 41]. In particular, Project ACHEON comprises thrust vectoring propulsive nozzle named HOMER (High Speed Orientating Momentum with Enhanced Reversibility) that is supported in a patent developed at University of Modena & Reggio Emilia [41].This system also comprises a plasma actuator (boundary layer control devices) that enables to extend vector range of operations of nozzle [45]

In the past, Germans used graphite control vanes in the exhaust stream of their V-2 ballistic missiles in World war 2 for some directional control of the jet [45]. Thrust vectoring in an aircraft is a relatively new practice and the concept came under use during cold war [45]. Several methods have been employed to generate thrust vectoring in the aircraft. Two common approaches have been taken to achieve thrust vectoring, namely mechanical and fluidic. Mechanical thrust vectoring uses turbofan engines with rotating nozzles or turning vanes to deflect the exhaust stream. This method can deflect thrust to as much as 90 degrees proving a vertical takeoff and landing capability. However, for vertical thrust the engine the aircraft requires a bigger heavier engine. As a result, there is increase in over all weight of aircraft and hence, the maneuverability reduced during the normal flight.

Alternatively, fluidic thrust vectoring approach has been proposed by several researchers [45]. In contrast to mechanical thrust vectors, fluidic thrust vector uses fixed geometry. In this approach, secondary flow has been used to control the main exhaust flow stream, and in this way redirect the flow at or near the exit plane. A wide range of concepts have been proposed such as shock vector control [70.], sonic throat skewing [69], synthetic jet actuator [70–71] and co-flow or counter flow [69] nozzles. Experiment tests concluded the main flow can be deflected up to 15^0. They are beneficial because they have around 50% lower mass and cost. Further, their inertia is lower thus making them faster to actuate which results in a stronger control response. Also, the complexity is reduced because they require mechanical simpler system with no moving parts, having also reduced radar cross section for stealth properties [45]. An excellent review of thrust vectoring approaches and its support in VTOL aircrafts has been presented by Pascoa et al. [45]. The throat shifting method is most efficient fluidic approach, but it requires to have the ability to control the throat area under various working conditions, which can be difficult. A large deflection angle is obtained in the shock vector control method, but can present problems associated to shock impingement and reflection. The co-flow thrust vectoring method is least efficient and has problems related to control reversal when low injections mass flow are applied . In case of counter flow method, problem may arise due to the availability of a suction system for the secondary flow. In view of this, a novel thrust vectoring approach ACHEON has been introduced [41, 44, 47]. It bears some resemblance with the co-flow, but it is not fluidic, and in this sense it will be less prone

to problems associated with the injection of low mass flows. In ACHEON, there is no secondary fluidic stream, but only two co-flow streams whose differential mass flow rated allows to control the thrust vector angle [41]. Plasma actuators will be implemented in HOMER nozzle to enhance and control the attachment of synthetic jet.

In the past, significant research on boundary layer control technologies, including active and passive flow controls, has been carried out. The main idea is to generate micro-vortex inside the boundary layer thickness, to add flow momentum close to the wall and to reduce separation. Flow control devices can be categorized in two group. Passive flow control devices, which do not add energy to air flow. These passive devices may be rendered mobile, thus increasing the range of aerodynamic optimization, but they are quite complex mechanisms which are heavy both in terms of weight and power consumptions. An alternative is to use active devices which add energy to air flow. These devices have been researched and shown their ability to control air flow for boundary layer separation, wing tip vortex, shock/boundary layer interaction, also for engine exhaust jet, landing gear and cavity noise reduction. Many active control devices have been proposed over the years [2]. A detailed review on active and passive flow control techniques can be found in [2–3].

Although the traditional methods of boundary layer control are effective from an aerodynamic point of view, their associated manufacturing and maintenance costs may limit their implementation, by introducing a significant increase in mechanical complexity and weight of the aircraft. Therefore, the replacement of these conventional systems by a system utilizing active flow control technology is a logical alternative. Plasma actuators are a relatively new flow control technology. A plasma actuator consists of two offset thin electrodes that are separated by a layer of dielectric insulator material. One of the electrodes is typically exposed to the air. The other electrode is fully covered by a dielectric material. The electrode exposed to air is assumed to be loaded by a high voltage, whereas an the electrode buried under dielectric is expected to be grounded. Comprehensive reviews on plasma on plasma actuators for aerodynamic flow controls have been published recently [3, 5]. Corke et al [4] provides an overview of the physics and modeling of SDBD (single dielectric barrier discharge) plasma actuators. It highlights some of the capabilities of plasma actuators through examples from experiments and simulations. Caruana [5] has given a survey of methods of air flow control for aircraft performance improvement. He has presented a short overview of non-plasma devices and studied ways for flow control. Touchard [6] also made a detailed review of the designs and associated setups for different aerodynamic plasma actuators developed these last twenty years, he further discussed the limits and the prospects of plasma actuators considered for airflow control.

In this work, a numerical investigation has been carried out on ACHEON system. Effect of plasma actuator has been studied on the system. Thrust vectoring characteristics such as thrust angle (θ_T) and thrust has been computed for different flow condtions. The performance of the nozzle has been obtained.

1.1 HOMER GEOMETRY AND OPERATION

In this section we will present the novel nozzle, describing its operation and presenting the numerical model approach employed.

The HOMER nozzle is depicted in Figure 1. The geometry comprises a duct (1) which bipartite into two channels by a central septum. The two channels converge into nozzle outlet, connected to Coanda surfaces (3) and (3´). This nozzle has an ability to permit the stabilization of a synthetic jet with arbitrary predefined direction and to modify this direction dynamically without any moving mechanical part. It generates a vectored and controllable

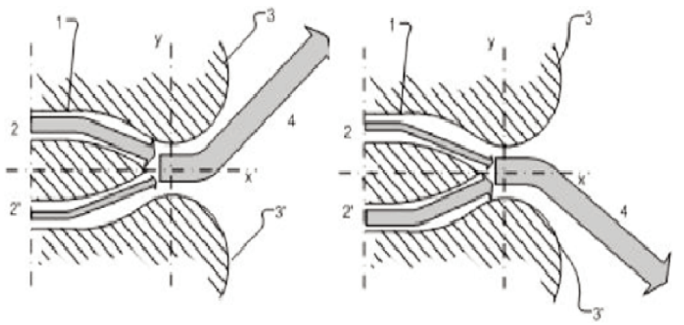

Figure 1: Geometry of the HOMER nozzle. It comprises two flow streams, feed by two electric turbofans, and an exit Coanda surface. Operation with different mass flows allows to control the exit flow angle.

jet by the combined action of two different physical phenomena: the mixing of two primitive jets (2) and (2´) and the angular deviation of the resulting synthetic jet by adhesion to the Coanda surfaces (3) and (3´).

Referring to Figure 1, the following conditions can be indentified:

1. If the momentum of the primitive jet (2) is greater than the one of (2´) the synthetic jet (4) adheres to Coanda surface designated as (3).
2. If the momentum of the primitive jet (2´) is greater than the one of (2) the synthetic jet (4) adheres to Coanda surface designated as (3´).
3. If momentums are equal the synthetic jet is aligned with the nozzle axis.

The angle formed by the synthetic jet (4) and the geometrical axis of the nozzle can be controlled by the momentums of primitive jets (2) and (2´). It can be increased when the difference between the moments of the two primitive jets (2) and (2´) increases, can be decreases and becomes null when it zero.

1.2 PLASMA ACTUATORS

Plasma-based devices exploit the momentum coupling between the surrounding gas and plasma to manipulate the flow. Unlike other flow control techniques, such as suction and mechanical actuators, plasma actuators require low power consumption, involve no moving mechanical parts, and have a very fast frequency response that allows real-time control. For these reasons, the plasma actuator has become a very promising and attractive device in the flow control community. Plasma actuators can be sub-categorized into two major families; the corona discharge, and the dielectric-barrier-discharge (the classification according to the class of discharges, may include corona discharge, dielectric barrier discharge (DBDs), glow discharge and arc discharge actuators; and also according to the conditions the classification can include the thermal and non-thermal plasma actuators). Different plasma actuators can be operated in various modes, depending on their geometrical configuration and the kind of high voltage applied (e.g., Nanosecond pulsed DBD, plasma synthetic jet, sliding DBD, Pulse DBD actuators). Very promising results for the application of plasma actuators have been observed in a wide range of aeronautic applications (boundary layer transition control [7], Separation control [8, 10], control of a subsonic rotor blade wake [11], increasing the lift on a UAV [12], noise reduction [13] and pressure sensor [14], elimination of low Reynolds number separation

in Low-Pressure Turbine flows [15] and reduction of the effects of turbine tip leakage [16]).

The specific plasma actuator which is considered for this study is the single-dielectric barrier-discharge (SDBD). In this configuration, two electrodes are typically separated by a dielectric barrier usually made of glass, Kapton or teflon as depicted in Figure 1. When a high AC voltage signal, of sufficient amplitude (5-40kVpp) and frequency (1-20 kHz), is applied between the electrodes the intense electric field partially ionizes the surrounding air, producing a nonthermal plasma on the dielectric surface. The collisions between the neutral particles and accelerated ions generate a net body force on the surrounding fluid. This body force is the mechanism for active aerodynamic control.

The advantages of DBD actuators include being surface-mounted (the ability to apply the actuators onto surfaces without the addition of cavities or holes), fully electronic, low power, high frequency-band devices, having a fast time response for unsteady applications, a very low mass and no moving parts. Moreover, flexible operation is possible by controlling the input voltage and waveforms. As DBD plasma actuators are thin, surface mounted, and do not require internal volumes or passages, they are particularly attractive for gas turbine and turbomachinery applications. Furthermore, plasma actuators like other active flow control devices can be driven either by open loop (not regulated by the output) or closed loop with feedback control [17] .

It has been observed that plasma actuators are sensitive to a variety of atmospheric conditions, including air velocity, humidity and air pressure, at which they are exposed in many potential practical applications. There have recently been a number of investigations into the effect of pressure and temperature (in other word gas density) on the body force and velocity profiles produced by DBD plasma actuators [18–27]. Although air pressure has effect on the current used by Dielectric Barrier Discharge (DBD) plasma actuators, and the voltage limits for plasma production, in this study as a first attempt that effect is not considered.

2. NUMERICAL METHOD

Initially, we performed two dimensional CFD calculations on nozzle geometries for various flow conditions (for low and higher speeds). The effect of plasma actuator has been studied on the nozzle. To characterize the thrust vectoring for the nozzle, performance parameter of the nozzle has been defined and studied under various flow conditions.

2.1. SOLUTION METHODOLOGY

2.1.1 Governing Equations

For the present case, we have considered a steady, two dimensional and incompressible flows in the nozzle. The governing equations can be written as vector form,

$$\nabla \bullet (\rho \vec{v}) = 0 \tag{1}$$

$$\nabla \bullet (\rho \overline{vv}) = -\nabla p + \nabla \bullet (\tau) + \rho \overline{g} + \overline{f}_b \tag{2}$$

The variables are ρ, $\vec{v}$, p, τ, $\vec{g}$ and $\vec{f}_b$ density, velocities, pressure, viscous shear stress tensor, acceleration due to gravity and body force respectively. For discretization of these equations, finite volume method has been used. 2nd order UPWIND scheme has been considered for the modeling of convective terms in the transport equations. Standard pressure interpolation scheme has been used for the pressure term in the equations. Moreover, for turbulent flow we have considered SST *k-w* model [31].

2.1.2 DBD Plasma Modeling

There have been several numerical studies on DBD plasma actuators. Two main different modeling approaches are commonly employed to describe the plasma actuators. The first consists of chemistry based models [32, 35] that attempt to spatially resolve the plasma phenomena directly. The second are algebraic models that are based on the solution of a Poisson's equation [36, 39], [10–11]. These algebraic models generally require assumptions regarding either the charge density or electric field produced by the actuator. The chemistry based family typically consists of drift diffusion type models. These models track the chemical species present in the plasma, such as electrons and ions, using a set of transport equations. The essential plasma physics such as ionization, recombination and streamer propagation are all modeled. Here in this study, the algebraic model of Suzen [39] is used for describing the effect of plasma actuation.

Split potential field model

The electrostatic formulation is based on the assumption that the plasma formation and fluid flow response can be decoupled due to the disparities in the characteristic velocities associated with each process. This is a reasonable assumption since the characteristic velocities of the transport fluid under consideration are between 10 m/s and 100 m/s and, for electron temperatures between 1000 K and 10000 K, the electron velocities, which present the characteristic velocities of the plasma, are of the order of 10^5–10^6 m/s.

The plasma actuators are formed by a pair of electrodes separated by a dielectric material. The actuator is placed in the surface with one electrode exposed to the surroundings and the other one embedded in the surface below the dielectric material (Figure 2).When a high AC voltage is supplied to the electrodes, this arrangement causes the air in their vicinity to weakly ionize. The ionized air, in the presence of the electric field gradient produced by the electrodes, results in a body force vector acting on the external flow that can induce steady or unsteady velocity components. This body force can be expressed in terms of the applied voltage and incorporated into the Navier Stokes equations. By neglecting magnetic forces, the electro hydrodynamic (EHD) force can be expressed as

$$\vec{f}_b = \rho_c \vec{E}, \tag{3}$$

where, $\vec{f}_b$ is the body force per unit volume, ρ_c is the net the charge density and $\vec{E}$ is the electric field. This body force is a body force per volume of plasma, which is the basis of the plasma actuator effect on neutral air. Considering the Maxwell equations (respectively Gauss law, Gauss law for magnetism, Faraday's law of induction and Ampere's circuital law) :

$$\Delta \bullet \vec{D} = \rho_c, \quad \Delta \bullet \vec{B} = 0, \quad \nabla \times \vec{E} = \frac{\partial \vec{B}}{\partial t}, \quad \nabla \times \vec{H} = \vec{J} - \frac{\partial \vec{D}}{\partial t}, \tag{4}$$

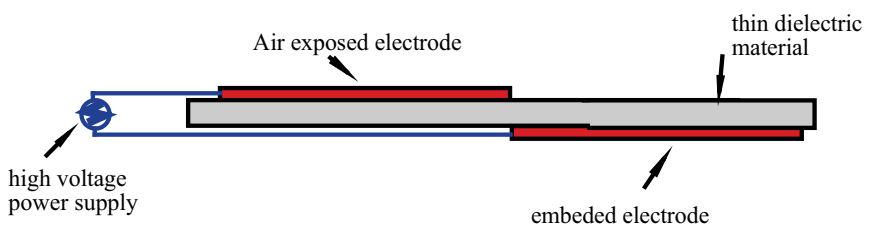

Figure 2: Schematic illustration of a single–dielectric barrier discharge plasma actuator

here $\vec{H}$ is the magnetic field strength, $\vec{B}$ is the magnetic induction, $\vec{E}$ is the electric field strength, $\vec{D}$ is the electric induction and $\vec{J}$ is the electric current. We assume that the charges in the plasma have sufficient amount of time for the redistribution process to occur and the whole system is quasi-steady, and that the time variation of the magnetic field is negligible, as is often the case in plasma. These assumptions imply that the electric current, $\vec{J}$, the magnetic field $\vec{H}$, and the magnetic induction $\vec{B}$ are equal to zero, as well as the time derivatives of the electric $\partial\vec{D}/\partial t$ and the magnetic induction, $\vec{B}/t$. Therefore, the Maxwell's equations give rise to

$$\Delta \bullet \vec{D} = \rho_c, \quad \Delta \times \vec{E} \approx 0, \tag{5}$$

The relation between the electric induction and the electric field strength is given by:

$$\vec{D} = \varepsilon \vec{E} \tag{6}$$

where ε is the permittivity. The permittivity can be expressed as $\varepsilon = \varepsilon_0 \varepsilon_r$ where ε_r is the relative permittivity of the medium, and ε_0 is the permittivity of free space. Using Eqn. (5), Eqn.(6) can be rewritten as,

$$\nabla \bullet \left(\varepsilon \vec{E}\right) = \rho_c, \quad \nabla \times \vec{E} \approx 0 \tag{7}$$

This implies that the electric field can be derived from the gradient of a scalar potential:

$$\vec{E} = -\nabla \Phi, \tag{8}$$

Therefore,

$$\nabla \bullet \left(\varepsilon_r \nabla \Phi\right) = -\frac{\rho_c}{\varepsilon_0}, \tag{9}$$

If we use the Boltzmann relation we have:

$$n_{e,i} = n_0 \exp\left(\pm \frac{e\varphi}{k_b T}\right) \approx n_0 \left[1 \pm \frac{e\varphi}{k_b T}\right] \tag{10}$$

with ϕ being the local electric potential, n_0 the background plasma density, T the temperature of the species, e the elementary charge, and K_b the Boltzmann constant. In the above equation, the positive sign applies to electrons and the minus sign applies to the ions. The net charge density at any point in a plasma is defined as the difference between the net positive charge produced by ions and the net negative charge of electrons. The difference can be related to the local electric potential ϕ by the Boltzmann relation (10). Assuming a quasi-steady state with a time scale long enough for the charges to redistribute themselves, the following relation can be written

$$\frac{\rho_c}{\varepsilon_0} = \frac{e}{\varepsilon_0}(n_i - n_e) \approx \frac{e n_0}{\varepsilon_0}\left(\exp\left(\frac{e\varphi}{k_b T_i}\right) + exp\left(\frac{e\varphi}{k_b T_e}\right)\right), \tag{11}$$

Where n_i and n_e being the ion and electron densities in the plasma. Expanding the exponential functions in a Taylor series for $\phi << T$, Equation (11) becomes, for the lowest order of φ/T,

$$\frac{\rho_c}{\varepsilon_0} \approx -\frac{e^2 \varphi n_0}{\varepsilon_0}\left(\frac{1}{k_b T_i} + \frac{1}{k_b T_e}\right), \tag{12}$$

The Debye length, which is the characteristic length for electrostatic shielding in a plasma, is defined as,

$$\lambda_d = \left[\frac{e^2 n_0}{\varepsilon_0} \left(\frac{1}{k_b T_i} + \frac{1}{k_b T_e} \right) \right]^{-\frac{1}{2}}, \tag{13}$$

The free charges in the plasma are shielded out in a distance given by the Debye length. The Debye shielding is valid if there are enough particles in the charge cloud. The criteria for this is the dimensionless plasma parameter, Δ, that characterizes un magnetized plasma systems, defined as

$$\Delta = \frac{4}{3} \pi \lambda_d^3 n_e , \tag{14}$$

If the plasma parameter is Δ>>1, then it means that the plasma is weakly-coupled, and the Debye shielding is valid. For plasma with the Debye length of approximately 0.00017 m, and the density of the charged particles is on the order of 10^{16} particles/m^3, the criteria is $\Delta = 3.5 \times 10^5$, indicating that the assumption of the Debye shielding is true. With the present definition of Debye length we have,

$$\frac{\rho_c}{\varepsilon_0} \approx -\frac{1}{\lambda_d^2} \Phi , \tag{15}$$

Experiments indicate that independently of which electrode the voltage is applied to, and independently of the polarity of the applied voltage, the resultant body force and the induced flow is in the direction towards the embedded electrode. The exposed surface of the dielectric plays a critical role. Even before the air ionizes, the dielectric surface communicates the potential charge from the covered electrode. When the voltage potential is large enough to ionize the air, the surface of the dielectric collects or discharges additional charge. As a result the dielectric surface is referred as a virtual electrode. Therefore there is the need for a better model that can account for these effects. According to [38] and [39] (split potential field model), since the gas particles are weakly ionized, we can assume the potential Φ can be decoupled into two parts: one being a potential due to the external electric field, ϕ, and the other being a potential due to the net charge density in the plasma, $\overline{\varphi}$,

$$\Phi = \overline{\varphi} + \phi \tag{16}$$

Assuming that the Debye length is small, and the charge on the wall above the encapsulated electrode is small, the distribution of charged particles in the domain is governed by the potential due to the electric charge on the wall, and is unaffected by the external electric field. Note that the grid spacing should not be larger than the Debye length. The smaller the Debye length, the narrower it becomes the plasma region located near the electrode and dielectric surface becomes. For the potential due to the external electric field, we have,

$$\nabla \bullet \left(\varepsilon_r \nabla \phi \right) = 0 \tag{17}$$

and for the potential due to the net charge density, we have,

$$\nabla \bullet \left(\varepsilon_r \nabla \overline{\varphi} \right) == -\frac{\rho_c}{\varepsilon_0} \tag{18}$$

Using Eqn. (15) we can rewrite Eqn. (18) as follows,

$$\nabla \bullet \left(\varepsilon_r \nabla \overline{\varphi}_c \right) = \frac{\rho_c}{\lambda_d^2}, \tag{19}$$

Equation (17) is solved for the electric potential, ϕ, using the applied voltage on the electrodes as boundary condition. The applied AC voltage is imposed at the exposed (upper) electrode as a boundary condition

$$\phi(t) = \phi_{\max} f(t), \tag{20}$$

The waveform function *f(t)*can be either a sine wave or a square wave given by,

$$\begin{aligned} &f(t) = sin(2\pi\omega t) \quad \textbf{(sine wave)}, \\ &f(t) = \begin{cases} 1; & sin(2\pi\omega t) n0 \\ -1; & sin(2\pi\omega t) < 0 \end{cases} \quad (square\ wave), \end{aligned} \tag{21}$$

where ω is the frequency and $\phi_{\max}$ is the amplitude. The embedded electrode is prescribed as ground by setting the electric potential to zero on that electrode. At the outer boundaries $\partial\phi / \partial n = 0$ is assumed. The waveform function *f(t)* is a time dependent boundary condition and can be used to model both steady and unsteady actuator arrangements. For the steady case, *f(t)* can be set to be a square wave. For unsteady cases, different frequencies and wave forms can be used to simulate actuation with different duty cycles. Eqn. (19) is solved for the net charge density ρ_c, only on the air side of the domain. A zero normal gradient for the net charge density is imposed on the solid walls except in the region covering the lower electrode. The charge density is set to zero on the outer boundaries. On the wall, downstream of the exposed electrode, where the embedded electrode is located (virtual electrode), the charge density is prescribed in such a way that it is matched with the time variation of the applied voltage $\phi(t)$on the exposed electrode,

$$\rho_{c,w}(t) = \rho_c^{\max} G(x) f(t), \tag{22}$$

where $\rho_c^{\max}$ is the maximum value of the charge density allowed in the domain (C / m^3). The variation of the charge density on the wall, $\rho_{c,w}$in the streamwise direction x, is prescribed by a function *G(x)* chosen to resemble the plasma distribution over the embedded electrode. Experimental results [40] suggest that this distribution is similar to a half Gaussian distribution given by

$$G(x) = exp(-(x - \mu)^2 / 2\sigma^2) \quad for \quad x \geq 0, \tag{23}$$

In eqn. (23) μ is the location parameter indicating the maximum x location, and σ is a scale parameter determining the rate of decay. The location parameter μ is chosen such that the peak corresponds to the left edge of the embedded electrode. Moreover, it is assumed that σ takes a value of 0.3 to allow a gradual decay of the charge density distribution from the left edge to the right edge. It should be noted that in order to solve the above equation, it is necessary to specify two parameters, namely $\rho_c^{\max}$ and λ_d These parameters control the strength of the plasma actuator's effects on the flow field and the extent of these effects into the flow field. These two parameters should be calibrated using available experimental data. The values for

ρ_c^{max} and λ_d were empirically defined by Suzen et al. (2005) [39] as 8×10^{-4} C/m^3, and 0.001m. Since Eqn. (17) and Eqn. (19) do not contain a time derivative term. Then, Eqn. (17) can be normalized using the value of voltage of the exposed electrode $\phi_{max} f(t)$, and be solved by imposing a constant boundary condition equal to unity at the upper electrode. Once the dimensionless distribution is determined, the dimensional values at any given time can be obtained by multiplying this distribution with the corresponding value of $\phi_{max} f(t)$. Similarly, equation (20) can be solved by normalizing with $\rho_c^{max} f(t)$. This implies that the boundary condition for the dimensionless charge density on the wall region covering the embedded electrode is $G(x)$. The non-dimensional form of Eqns. (17) and (19) is as follows,

$$\nabla \bullet \left(\varepsilon_r \nabla \phi^*\right) = 0, \quad \phi^* = \frac{\phi}{\phi_{max} f(t)}, \tag{24}$$

$$\nabla \bullet \left(\varepsilon_r \nabla \rho_c^*\right) = \frac{\rho_c^*}{\rho_d^2}, \quad \rho_c^* = \frac{\rho_c}{\rho_c^{max} f(t)}, \tag{25}$$

2.1.3 Computational Grid

Figure 3 shows the computational grid for the numerical simulation. In order to capture the boundary layer effects near Coanda surface, y+< 1 was considered. 2, 18, 155 hexahedral mesh was created using commercial mesh generation tool Pointwise. For modeling of Plasma near Coanda surface (Figure 3), an electrode with length 10 mm with thickness 1mm is mounted on Coanda surface. Another electrode with the same thickness and 1 mm in length is grounded and separated from the mounted electrode with the 3 mm thick layer of kapton as dielectric material. For the present simulation, three plasma actuators have been used.

A commercial package FLUENT [50] has been used for the simulation. A user defined functions (UDF) has been coded and used for calculations of electric field and body force. Various types of boundary conditions have been used for the computation. Velocity inlet conditions have been considered at the both the inlet section of nozzle. Pressure outlet boundary conditions have been used as the outlet boundary conditions. The convergence of the numerical solution has been checked through the convergence history of lift and drag coefficient inside the nozzle.

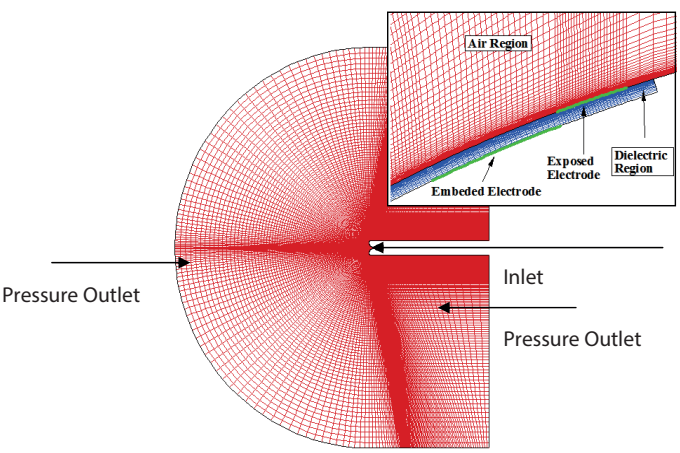

Figure. 3: Computational grid for numerical simulation

3.RESULTS AND DISCUSSION

First, CFD calculations have been done for different velocity ranges without plasma actuators.

Table 1 and Table 2 show the different test cases for the numerical computation of the nozzle without plasma. Where, VR is the velocity ratio between two inlet (Figure 1) velocities. T_x and T_y are the magnitude of thrust in x and y direction respectively. θ_T and T_{max} are the thrust vectoring angle and maximum thrust. α is the jet vectoring angle for the jet. Simulations have been performed in the range of maximum velocities (V_{max}), 14 m/s to 80 m/s. Velocity contour for velocity ratio (VR) = 1.2 has been shown in figure 4.

Table 1: For low speed flows (without Plasma)

V_{max}	VR	Ty/Tx	θ_T	α	T_{max}
14.378	1.2	0.293	16.55	24.46	5.35
16.45	1.4	0.744	28.36	34.33	7.59
21.91	2.0	0.731	36.16	47.01	15.85
24.42	0.0	0	0	0	15.134

Table 2: For high speed flows (without Plasma)

V_{max}	VR	Ty/Tx	θ_T	α	T_{max}
54.70	1.2	0.7202	36.06	47.31	96.55
64.60	1.4	0.7684	37.53	54.46	172.99
80.54	2.0	0.6709	33.85	73.27	332.024

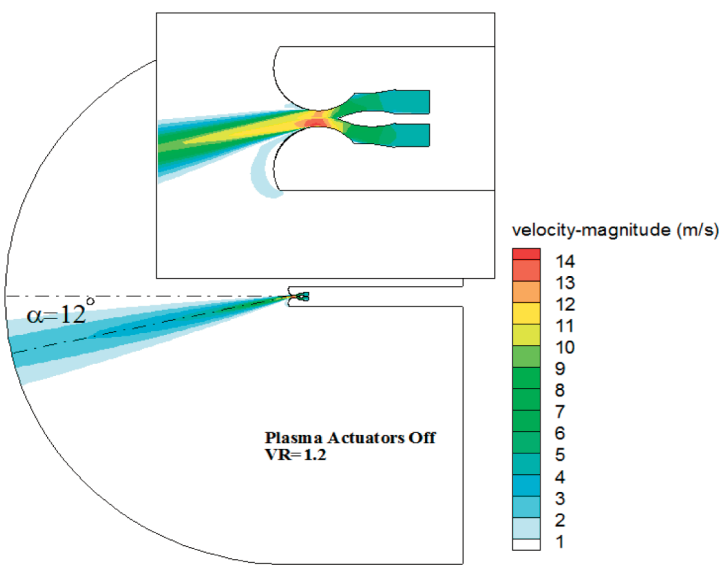

Figure 4: Velocity contour for VR = 1.2 without Plasma

In a subsequent, CFD calculations were performed for both low and high speed flows in the presence of plasma actuor on inside the nozzle. The distribution of electric potential and charge density around the electrodes near Coanda surface is shown in Figure. 5. As shown in Figure 6, the presence of potential difference between the electrodes, the air ionizes and forms ionic wind. This ionic wind overcome the adverse pressure gradient near Coanda surface and delays the flow separation. The presence of plasma actutaor near Coanda surface significantly increases the jet deflection angle (Figure 7.).

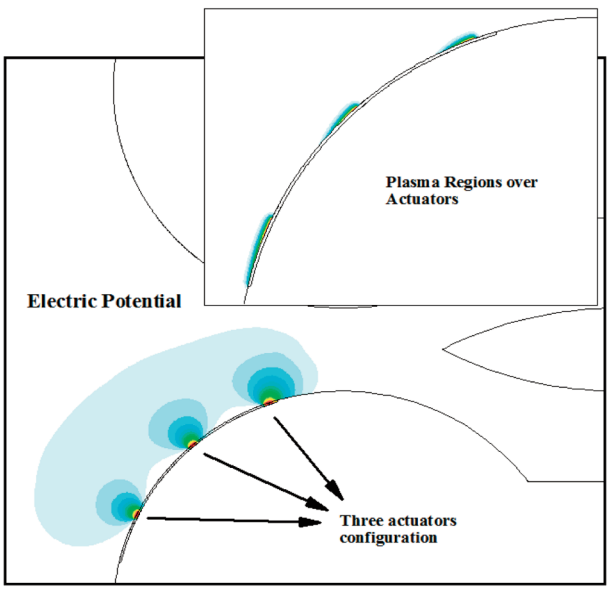

Figure 5: Plasma actuators

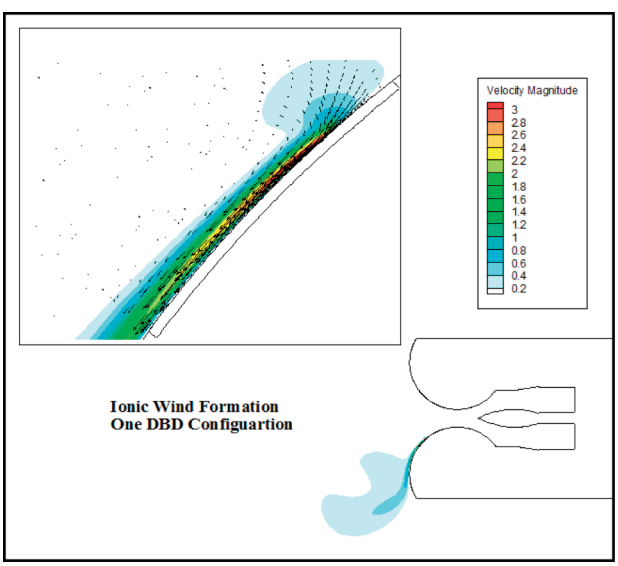

Figure 6: Ionic wind formation

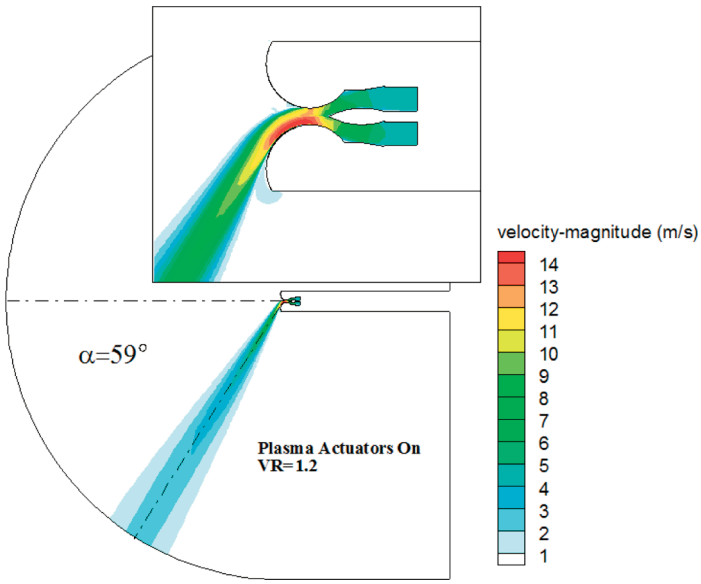

Figure 7: Velocity contour for VR = 1.2 with Plasma

Table 3: For low speed flows (with Plasma)

V_{max}	VR	Ty/Tx	θ_T	α	T_{max}
15.04	1.2	0.718	35.57	57.20	10.32
16.79	1.4	0.744	36.644	54.11	12.323
21.98	2.0	0.669	36.16	65.75	20.84
25.92	0.0	0.669	33.78	46.96	22.52

Table 4: For high speed flows (with Plasma)

V_{max}	VR	Ty/Tx	θ_T	α	T_{max}
54.82	1.2	0.7601	37.23	52.15	106.25
61.30	1.4	0.7783	37.89	54.77	155.61
80.36	2.0	0.731	33.91	75.97	332.04

Table 3 and Table 4 show the different test cases for the numerical computation of the nozzle with plasma.

For lower speed flows, the jet deflection angle (α) increases with increase in velocity ratio´s (VR) (Table 1). The variation of thrust vectoring angle (θ_T) and maximum thrust (T_{max}) with VR is presented in Figure 8 and Figure 9. As it clear from Figure 8., θ_T increases with increase in VR's. It is interesting to note that, θ_T improves significantly for the lower speed flows with the plasma on (Figure 8). It is clear from Figure 9, T_{max} decreases with increase in velocity ratio (VR) from 0 to 1.2, then it increases towards higher VR's. In the presence of plasma, the thrust magnitude for the nozzle has been raised (Figure 9). It means,

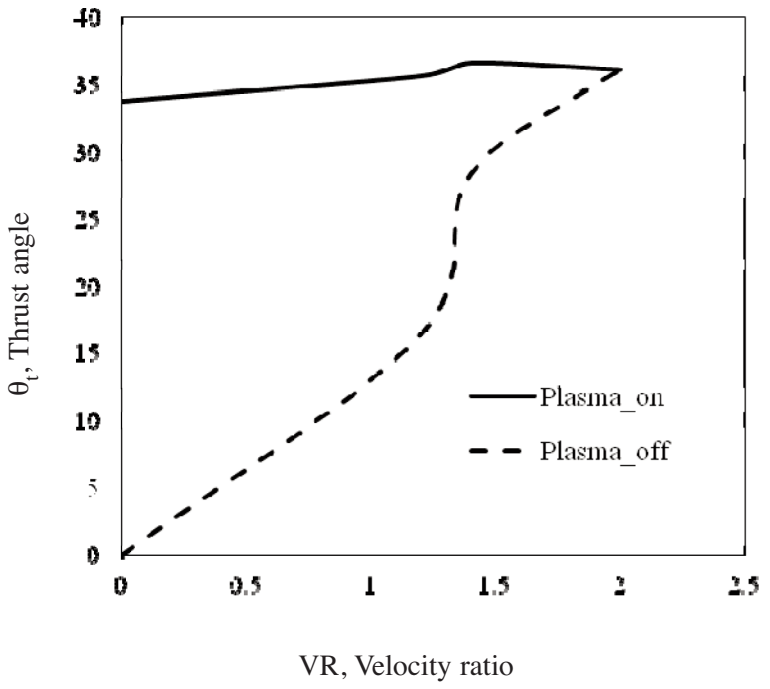

Figure 8: Low speed flows: Variation of thrust angle (θ_T) with velocity ratio (VR) with and without Plasma

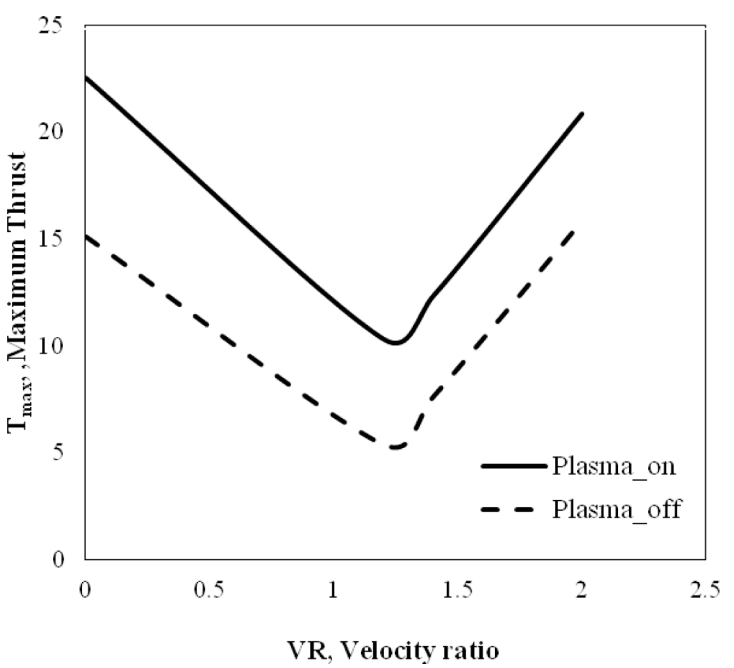

Figure 9: Low speed flows: Variation of maximum thrust (T_{Max}) with velocity ratio (VR) with and without Plasma

with less power consumption, the efficiency of the nozzle has been enhanced with use of plasma actuators.

For high speed flows, it was observed that α increases with increase in VR's (Table 2). It is clear from figure 10, that θ_T decreases with increase in VR's. It is interesting to note that, the effect of plasma is less significant the the variation of θ_T with VR for high speed flows.

It is clear from figure 11, for high speed flows, θ_T increases with increase in of VR. The effect of plasma on the thrust vectoring for the nozzle is less for higher velocity ratio in case of high speed flows. From above study, it may be concluded that, there is an upper limit for vectoring thrust angle for the high speed flows with and without plasma actuators.

The thrust vectoring for the nozzle, can be characterized by defining performance parameter (PP) of the nozzle

$$PP = (\theta_T)/((m_2)/(m_2+m_{2'})) \tag{26}$$

Where, m_2 and $m_{2'}$ are the mass flow rate in inlet 2 and inlet 2´ of the nozzle (Figure 1).

The performance parameter (PP) of the nozzle for both lower and higher speed flows is shown in Figure 12 A and B. It has been observed that, for the lower speed flows the performance of the nozzle improves significantly in the presence of plasma actuator. In contrast, the effect of plasma is less significant for high speed flows.

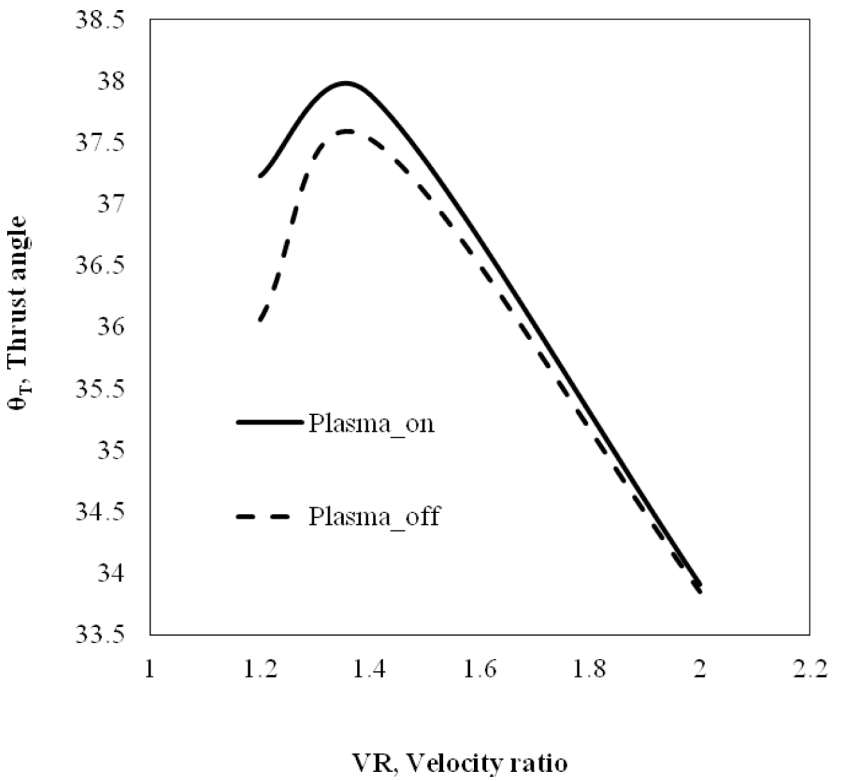

Figure 10: High speed flows: Variation of thrust angle (θ_T) with velocity ratio (VR) with and without Plasma

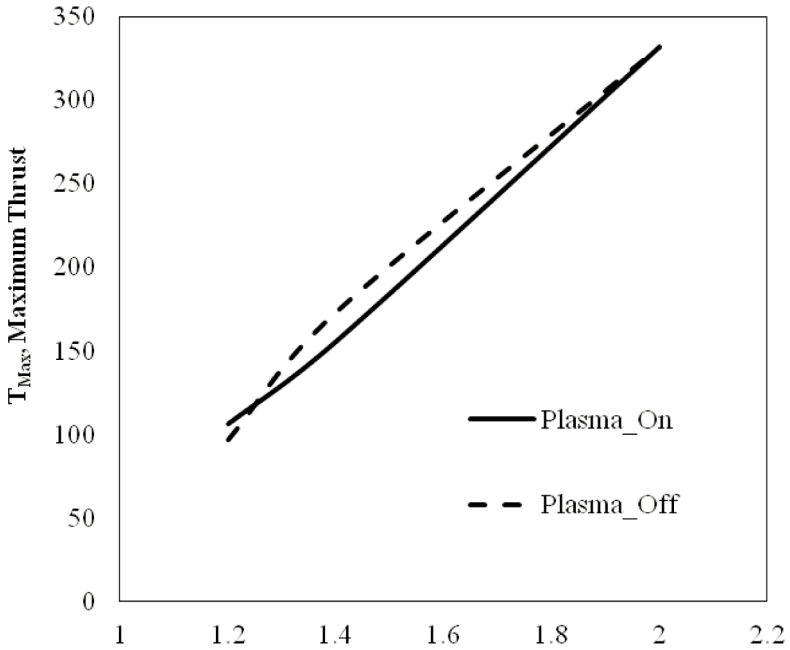

Figure 11: High speed flows: Variation of maximum thrust (T_{Max}) with velocity ratio (VR) with and without Plasma

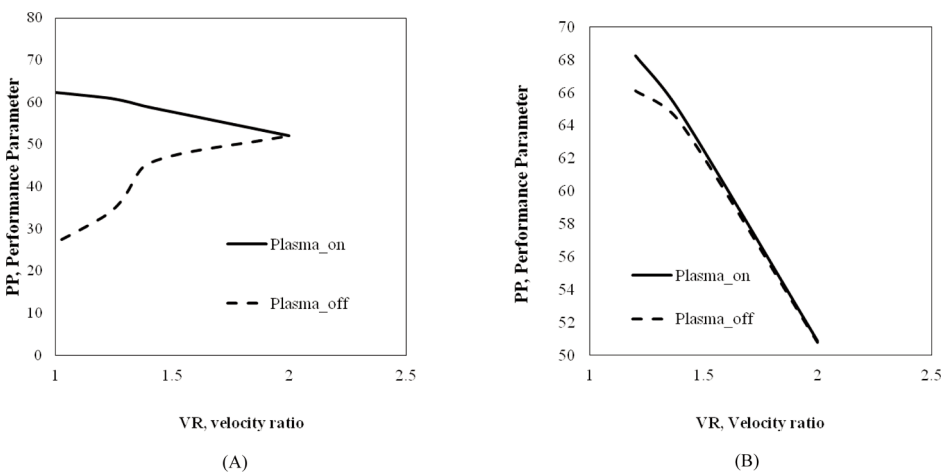

Figure. 12: Performance parameter (A) low speed flows (B) High speed flows

4. CONCLUSION

A computational study on newly proposed propulsion system ACHEON has been conducted. Two dimensional, incompressible, Reynolds-averaged Navier Stokes eqns. has been solved with simple electrostatic model to simulate flow inside the nozzle. The innovative active flow control of plasma actuators has been considered near Coanda surface. It has been observed from above study, plasma actuators are very effective in case

of low speed flows. From, the numerical result it can be concluded that, the plasma actuators have an potential to enhance the performance of the nozzle for lower speed flows (less power consumption).

ACKNOWLEDGEMENTS

The present work was partial supported by European project ACHEON (Aerial Coanda High Efficiency Orienting jet Nozzle) under Contract N 309041 of the 7th Framework of Programme and by FCT-Research Unit No. 151

REFERENCES

[1] ACHEON, "Acheon project," 2013. [Online]. Available :http://acheon.eu/project/.

[2] L. N. Cattafesta III, M. Sheplak: Actuators for Active Flow Control. Annual Review of Fluid Mechanics, 43(2011), 247-272.

[3] M. Gad-El-Hak, *Flow Control: Passive, Active, and Reactive Flow Management*. New York: CambridgeUniversity Press, 2000.

[4] Thomas C. Corke, C. Lon Enloe, Stephen P. Wilkinson: Dielectric Barrier Discharge Plasma Actuators for Flow Control. *Annu. Rev. Fluid Mech*., 42(2010), 505–29.

[5] D Caruana : Plasmas for aerodynamic control. *Plasma Phys. Control. Fusion*, 52(2010), 124045.

[6] G. Touchard: Plasma actuators for aeronautics applications - State of art review-. *International Journal of Plasma Environmental Science and Technology*, 2(2008).

[7] R. Hanson, P. Lavoie, A. Naguib, J. Morrison: Transient growth instability cancellation by a plasma actuator array. *Experiments in Fluids*, 49(2010)1339–1348.

[8] T. Corke, M. Post, D. Orlov : SDBD plasma enhanced aerodynamics: concepts, optimization and applications. *Progress in Aerospace Sciences*,43(2007)212–217.

[9] D. M. Orlov, T. Apker, C. He, H. Othman, T.C. Corke : Modeling and Experiment of Leading Edge Separation Control Using SDBD Plasma Actuators. in *AIAA 45th Aerospace Sciences Meeting AIAA paper No. 2007–0877*, Reno, Nevada, 8–11 January 2007.

[10] D. M. Orlov: Modeling and simulation of single dielectric barrier discharge plasma actuators. University of Notre Dame, Ph.D. thesis 2006.

[11] S. Lemire, H.D. Vo : Reduction of fan and compressor wake defect using plasma actuation for tonal noise reduction. *Journal of Turbomachinery*, 133(2011)

[12] S. Grundmann, M. Frey, C. Tropea : Unmanned aerial vehicle (UAV) with plasma actuators for separation control. in *47th AIAA Aerospace Sciences Meeting Including the New Horizons Forum and Aerospace Exposition in Orlando Florida*, 2009, p. 698.

[13] F. Thomas, A. Kozlov, T. Corke : Plasma actuators for cylinder flow control and noise reduction. *AIAA Journal*, 46(2008), 1921–1931.

[14] Monique M. Hollick, Maziar Arjomandi, Benjamin S. Cazzolato:An investigation into the sensory application of DBD plasma actuators for pressure measurement. *Sensors and Actuators A*, 171(2011), 102–108.

[15] J. Huang, T.C. Corke, and F.O. Thomas: Unsteady Plasma Actuators for Separation Control of Low-PressureTurbine Blades. *AIAA Journal*, 44(2006), 1477–1487.

[16] S.C. Morris, T.C. Corke, D. VanNess, J. Stephens, T. Douvillev: Tip Clearance Control Using Plasma Actuators. *AIAA–2005–782*, 2005.

[17] Young-Chang Cho, Wei Shyy: Adaptive flow control of low-Reynolds number aerodynamics using dielectric barrier discharge actuator. *Progress in Aerospace Sciences*, 47(2011) 495–521.

[18] E. Matlis, T. Corke, S. Gogineni : A.C. plasma anemometer for hypersonic Mach number experiments. *AIAA*, pp. 2005-0952, 2005.

[19] T. Abe, Y. Takizawa, S. Sato : A parametric experimental study for momentum transfer by plasma actuator. *AIAA Journal*, pp. 2007-0187, 2007.

[20] N. Benard, N. Balcon, E. Moreau, "Electric wind produced by a surface dielectric barrier discharge operating in air at different pressures: Aeronautical control insights. *Journal of Physics D: Applied Physics*, 41(2008), 042002

[21] P. Versailles, V. Gingras-Gosselin, V. Duc : Impact of pressure and temperature on the performance of plasma actuators. *AIAA Journal*, 48(2009), 859-863.

[22] B. Chartier, M. Arjomandi, B. Cazzolato: An investigation on the application of DBD plasma actuators as pressure sensors . *AIAA Proceedings*, p. 092407, 2009.

[23] Timothy G. Nichols, Joshua L. Rovey: Fundamental Processes of DBD Plasma Actuators Operating at High Altitude. in *50th AIAA Aerospace Sciences Meeting including the New Horizons Forum and Aerospace Exposition*, Nashville, Tennessee, 09 - 12 January 2012, pp. AIAA 2012-0822.

[24] Joseph A. Valerioti, "Pressure Dependence of Plasma Actuated Flow Control," University of Notre Dame, Notre Dame, Indiana, Mater thesis 2010.

[25] James W. Gregory, C. Lon Enloe, Gabriel I. Font, Thomas E. McLaughlin: Force Production Mechanisms of a Dielectric-Barrier Discharge Plasma Actuator. in *45th AIAA Aerospace Sciences Meeting and Exhibit AIAA 2007-185*, Reno, Nevada, 8–11 January 2007.

[26] N. Benard, E. Moreau: Effects of Altitude on the Electromechanical Characteristics of Dielectric Barrier Discharge Plasma Actuators. *AIAA–2010–4633*, 2010.

[27] G.I. Font et al., "Effects of Oxygen Content on the Behavior of the Dielectric Barrier Discharge Aerodynamic Plasma Actuator," *AIAA–2010–545*, 2010.

[28] A Arnone, M.S. Liou, L.A. Povineli: Multigrid calculation of three-dimensional viscous cascade flow. NASA Technical Memorandum 10-5257 1991.

[29] P.L. Roe: Approximate Riemann solver, parameters vectors and difference schemes. *J. Comp. Phys.*, 43(1981)357–371.

[30] E. Toro, *Riemann solvers and numerical methods for fluid dynamics*. New York: Springer-Verlag, 1999.

[31] D.C. Wilcox, *Turbulence Modeling for CFD*. 5354 Palm Drive, La Canada, California: DCW Industries, Inc., 1993.

[32] K. Singh, S. Roy: Modeling plasma actuators with air chemistry for effective flow. *J. Appl. Phys,* vol. 101, 2007.

[33] B. Jayaraman: Computational modeling of glow discharge-induced fluid dynamics. University of Florida, Ph.D. thesis 2006.

[34] A. Likhanskii, M. Shneider, S. Macheret, and R. Miles: Modeling of dielectric barrier discharge plasma actuators driven by repetitive nanosecond pulses. *Physics of Plasmas*, vol. 14, 2007.

[35] Xueke Che, Tao Shao, Wansheng Nie, Ping Yan :Numerical simulation on a nanosecond-pulse surface dielectric barrier discharge actuator in near space. *J. Phys. D: Appl. Phys*., 45(2012),145201.

[36] W. Shyy, B. Jayaraman, A. Andersson: Modeling of glow discharge-induced fluid. *J. Appl. Phys*., 92(2002), 6434–6443.

[37] B.E. Mertz: refinement, validation, and implementation of lumped circuit element model for single dielectric barrier discharge plasma actuators. University of Notre Dame, Ph.D. thesis 2010.

[38] Y. B. Suzen P. G. Huang: Simulations of Flow Separation Control using Plasma Actuators. Reno, Nevada, 9–12 January 2006, p. 44th AIM Aerospace Sciences Meeting and Exhibit.

[39] Y. B. Suzen, P. G. Huang, J. D. Jacob, D. E. Ashpis : Numerical Simulations of Plasma Based Flow Control Applications. in *35th Fluid Dynamics Conference and Exhibit AIAA, AIAA 2005-4633*, Toronto, Ontario, June 6–9, 2005, p. 4633.

[40] C.L., McLaughlin, T.E., VanDyken, R.D., Kachner, K.D., Jumper, E.J., Corke, T.C., Post, M. Haddad, O. Enloe: Mechanisms and Responses of a Single Dielectric Barrier Plasma Actuator: Geometric Effects. *AIM Journal*, vol. 42, no. 3, pp. 595-604, March 2004.

[41] Trancossi, M. and Dumas, A., "A.C.H.E.O.N.: Aerial Coanda High Efficiency Orienting-jetNozzle," SAE Technical Paper 2011-01-2737, 2011, doi:10.4271/2011-01-2737.

[42] Newman, B. G., The Deflexion of Plane Jets by Adjacent Boundaries, in Coanda Effect, Boundary Layer andFlow Control, edited by G. V. Lachmann, Vol. 1, Pergamon Press, Oxford, 1961, pp. 232-264.

[43] Saeed, B., Gratton, G., and Mares, C., "A Feasibility Assessment of Annular Winged VTOL Flight Vehicles,"The Aeronautical Journal, 115:683–692, 2011.

[44] Trancossi, M., "An Overview of Scientific and Technical Literature on Coanda Effect Applied to Nozzles,"SAE Technical Paper 2011-01-2591, 2011, doi:10.4271/2011-01-2591.

[45] Pascoa J., Dumas A. and others, A review of thrust-vectoring in support of a V/STOL non-moving mechanical propulsion system, Central European Journal of Engineering, Volume 3, Issue 3, pp 374-388, 2013.

[46] Trancossi, M. and Dumas, A., "Coanda Synthetic Jet Deflection Apparatus and Control," SAE Technical Paper 2011-01-2590, 2011, doi:10.4271/2011-01-2590.

[47] Trancossi M., Subhash M., Angeli D., "Mathematical modelling of a two streams Coanda effect nozzle" –ASME International Mechanical Engineering Conference and Exhibition, paper n. IMECE2013-63459, 2013.

[48] Subhash, M. and Dumas, A., "Computational Study of Coanda Adhesion Over Curved Surface," SAE paper no:2013-01-2302 (in press).

[49] Suñol, D. Vucinic, M. A. Bidakhvidi, S. Vanlanduit CFD MODELING OF THE COANDA BASED THRUST VECTORING NOZZLE, ACEX-2013, Madrid, Spain VV.AA., Fluent 6.3 and Gambit User manual, 2008.

[50] Patankar, S. V., "Numerical Heat Transfer and Fluid Flow," Hemisphere, Washington, DC, 1980.

[51] Schlichting, H., Gersten, K., and others, "Boundary-Layer Theory" 8th edition Springer 2004

[52] Yoshitani, N., Hashimoto, S-I., Kimura, T., Motohashi, K., Ueno, S., " Flight Control Simulators for Unmanned Fixed-Wing and VTOL Aircraft", ICROS-SICE International Joint Conference 2009, August 18-21, 2009, Fukuoka International Congress Center, Japan.

[53] Hennissen, J., Temmerman, W., Berghmans, J., and Allaert., K. " Modelling of Axial Fans for Electric Equipment". EUROTHERM SEM. no. 45, 1995.

[54] Ilieva G., Páscoa J.C., Dumas A., Trancossi M. (2012), "A critical review of propulsion concepts for modern airships", Central European Journal of Engineering, Vol. 2(2), pp. 189-200, DOI:10.2478/s13531-011-0070-1.

[55] Páscoa J. C., Mendes A. C., Gato L.M.C. (2009), "A fast iterative inverse method for turbomachinery blade design", Mechanics Research Communications, Vol. 36(5), pp. 537-546.

[56] Trancossi, M., Madonia, M., "The Efficiency of an Electric Turbofan vs. Inlet Area: A Simple Mathematical Model and CFD Simulations," SAE Technical Paper 2012-01-2217, 2012, doi:10.4271/2012-01-2217.

[57] M. Trancossi, "An Overview of Scientific and Technical Literature on Coanda Effect Applied to Nozzles," SAE Technical Paper 2011-01-2591, 2011, doi:10.4271/2011-01-2591.

[58] M. Trancossi, and A. Dumas, "Coanda Synthetic Jet Deflection Apparatus and Control," SAE Technical Paper 2011-01-2590, 2011, doi:10.4271/2011-01-2590.

[59] J. C. Páscoa, A. Dumas, M. Trancossi, P. Stewart, D. Vucinic, "A review of thrust-vectoring in support of a V/STOL non-moving mechanical propulsion system", Central European Journal of Engineering, September 2013, vol. 3, Issue 3, pp 374-388, doi: 10.2478/s13531-013-0114-9.

[60] M. Trancossi, S. Maharshi, D. Fregni, "Mathematical modelling of a two streams Coanda effect nozzle", SAE International Journal of Aerospace, Vol. 6, No.1: September 2013.

[61] Subhash, M. and Dumas, A., "Computational Study of Coanda Adhesion Over Curved Surface", SAE International Journal of Aerospace, Vol. 6, No.1: September 2013, doi:10.4271/2013-01-2302.

[62] M. Trancossi, A. Dumas, D. Vucinic, "Mathematical Modeling of Coanda Effect", Paper No: 2013-01-2195, SAE International Journal of Aerospace, Vol. 6, No.1: September 2013.

[63] M. Trancossi; J. Pascoa, "ThermoJet an Old Concept Which Can Prelude a Future Green Air Transport", Paper No: 2013-01-2205, SAE International Journal of Aerospace, Vol. 6, No.1: September 2013.

[64] F. Grimaccia, "Regulatory and standardization for unconventional aircraft in light UAV segment", Paper Number: 2013-01-2103, SAE International Journal of Aerospace, Vol. 6, No.1: September 2013.

[65] Trancossi M., Subhash M. Angeli D., Mathematical modelling of a two Streams Coanda effect Nozzle, Proceedings of IMECE2013, IMECE2013-63459,to be published ASME International Mechanical Engineering Congress and Exposition, November 15-21, San Diego, California, USA.

[66] A. Dumas, M. Trancossi, S.Maharshi, J.M.Pascoa, "The Influence of Surface temperature on Coanda Surface", Energy Procedia (An Elsevier Journal).

[67] B. Saeed, G. Gratton, and C. Mares, "A feasibility assessment of annular winged VTOL flight vehicles," The Aeronautical Journal, vol. 115, pp. 683–692, 2011.

[68] AGARD, "V/STOL handling i-criteria and discussion," Tech. Rep. AGARD-R-577-70, Advisory Group for Aerospace Research & Development, 1970.

[69] E. MORALEZ, V. MERRICK, and J. SCHROEDER, "Simulation evaluation of an advanced control concept for a V/STOL aircraft," journal of Guidance Control and Dynamics, vol. 12, pp. 334–341, 1989.

[70] R. Naldi and L. Marconi, "Optimal transition maneuvers for a class of V/STOL aircraft," Automatica, vol. 47, pp. 870–879, 2011.

[71] P. Strykowski and A. Krothapalli, "An experimental investigation of active control of thrust vectoring nozzle flow fields," tech. rep., The University of Minnesota, 1993.

[72] M. Mason and W. Crowther, "Fluidic thrust vectoring of low observable aircraft," in CEAS Aerospace Aerodynamic Research Conference, pp. 1–7, 2002.

[73] D. Wing, "Static investigation of two fluidic thrust-vectoring concepts on a two-dimensional convergent-divergent nozzle," Tech. Rep. TM-4574, NASA Langley Research Center, 1994.

[74] M. Abdollahzadeh, J. Páscoa, P.J. Oliveira, Numerical investigation on efficiency increase in high altitude propulsion systems using plasma actuators,in: ECCOMAS European Congress on Computational Methods in Applied Sciences and Engineering, 2012, pp. 6563–6581.